Super-Resolution Reconstruction of Plane-Wave Ultrasound Imaging Based on the Improved CNN Method

Zixia Zhou[1], Yuanyuan Wang[1,2(✉)], Jinhua Yu[1,2], Wei Guo[1], and Zhenghan Fang[1]

[1] Department of Electronic Engineering, Fudan University, Shanghai, China
yywang@fudan.edu.cn
[2] Key Laboratory of Medical Imaging Computing and Computer Assisted Intervention
of Shanghai, Fudan University, Shanghai, China

Abstract. Plane wave imaging (PWI) can cover the entire image region by using a single plane wave transmission. The time-saving imaging mode, however, provides poor imaging resolution and contrast. It is highly demanded for the PWI to compensate the weakness in the imaging quality while maintain the ultrafast imaging speed. In this paper, we proposed a multi-scaled convolutional neural network (CNN) model to improve the quality of the PWI. To further increase the convergence rate and robustness of the CNN, a feedback system was added into the iteration process of the stochastic parallel gradient descent (SPGD) optimization. Three different types of data including the simulation, phantom and real human data have been used in the experiment with each class containing 150 pairs of data. The proposed method produced 52% improvement in the peak signal to noise ratio (PSNR) and 4 times improvement in the structural similarity index measurement (SSIM) compared with the original images. Moreover, the proposed method not only guarantees the global convergence, but also improves the converging rate with 15% reduction of the total elapsed time.

Keywords: Ultrasound imaging · Plane wave · Super-resolution reconstruction · Deep learning · Convolutional neural network (CNN) · Feedback system

1 Introduction

As an important ultrasound imaging mode, plane-wave imaging (PWI) can get the entire imaging data by just one emission. This mode greatly reduces the number of emission in the traditional line-by-line scanning and improves the imaging frame rate considerably. The PWI usually has high temporal resolution and is suitable for three-dimensional real-time imaging. On the other hand, because of the unfocused plane-wave beam, the PWI has the problems of high noise and low signal-to-noise ratio, resulting in the degraded image resolution and contrast. The poor imaging quality of the PWI limits its development and clinical usage. Many methods have been proposed to improve the quality of the PWI while maintain its high temporal resolution. These methods can be divided into two groups: the adaptive beamforming methods [1, 2] and super-resolution reconstruction based on the post image processing [3, 4]. Different from beamforming methods that work on the raw radio-frequency (RF) signals during the imaging process,

the super-resolution reconstruction restores an image with the improved spatial resolution by the post image processing. Traditional super-resolution methods include the interpolation method [5], the wavelet method [6], the maximum likelihood method [7], the sparse representation method [8], and etc. Nevertheless, the huge computation and complex algorithm are the limitations of these methods.

Recently, deep learning is an intensively researched topic in the field of computer vision and image processing. Deep learning brings a considerable improvement in many traditional issues including image segmentation, registration, and classification. Besides, it has also been proposed by using deep learning methods to improve the image quality. They were applied in many fields ranging from remote sensing to medical imaging. As one of widely used deep learning methods, the convolutional neural network (CNN) imitates the working pattern of human brain and does not need to detect features manually. These properties make the CNN a promising option in the field of super-resolution image reconstruction. For instance, Dong et al. [9] proposed a lightweight structure deep CNN for the single image super-resolution which directly learns an end-to-end mapping between the low/high-resolution images for the first time. In order to improve the effectiveness and efficiency of the reconstruction process, Kim et al. [10] presented a highly accurate single-image super-resolution (SR) method in which a very deep convolutional network was used. In addition, some medical image super-resolution methods were proposed such as compensating the resolution difference between 3T MRI and 7T MRI with a CNN algorithm in Bahrami et al. [11].

In this paper, we apply a novel CNN model for ultrasound plane-wave images super-resolution reconstruction. Firstly, a multi-scaled CNN model, which aims to improve the quality of image details and textures, is introduced. Secondly, different types of data including the simulation, phantom and real human data are chosen for CNN training to guarantee the generality of the application. In order to solve the convergence problem of the CNN under large amounts of data (100 million pairs of patches in all), a feedback system is proposed to improve the convergence speed during training. Finally, the results have evaluated with five performance measurements.

Overall, the main contributions of this study are to expand the applicable range of the CNN super-resolution reconstruction method to ultrasound plane-wave images and present a novel CNN structure on the specific application with satisfactory results.

2   Materials and Methods

2.1   Materials

The simulation images were chosen to generate an ideal experiment condition. As shown in Fig. 1, the simulation images including 75 pairs of point (a), (g) and 75 pairs of cyst (b), (h). The point object images have the length of 0.098 mm per horizontal pixel. All simulation images were generated by the ultrasound simulation program Field_II.
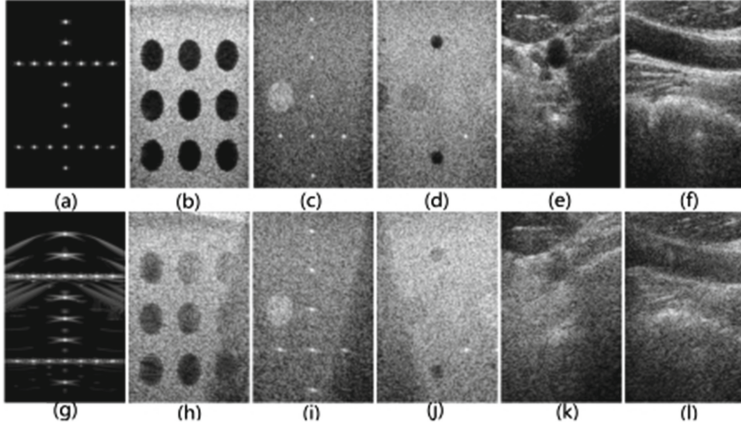
Fig. 1. Image data of the reconstruction experiments. The first row: high resolution, second row: low-resolution training samples.

The phantom images were obtained to get more realistic results. As shown in Fig. 1(c), (d), (i) and (j), two locations of phantom were scanned with Verasonics vantage system (each has 75 pairs of images). The multi-tissue model 040GSE phantom was produced by the Computerized Imaging Reference Systems (CIRS).

The real human images were also studied for the practical application. 75 pairs of thyroid gland ultrasound images and 75 pairs of carotid artery ultrasound images were selected as displayed in Fig. 1(e), (f), (k) and (l).

All images have 387×609 pixels in dimensions. Each training pair contains a single-angle low-resolution patch and the corresponding multi-angle high resolution patch. The high resolution images were synthesized by three different beamforming methods: the delay-and-sum (DAS) beamformer, the minimum variance (MV) based beamformer, and the eigenspace based minimum variance (ESBMV) beamformer with 75 different scanning angles. The public datasets provided by the plane wave imaging challenging in medical ultrasound (PICMUS) [12].

2.2   CNN Model

As shown in Fig. 2, three CNN models (the model (a), (b) and (c)) were used to the point and cyst simulation images so that the most suitable CNN model for these two specific object ultrasound images could be found. After that, we made use of a multi-scale real-time feedback structure to the phantom images and real human images, the overall picture in Fig. 2 describes this structure which combined with three different scale network models.
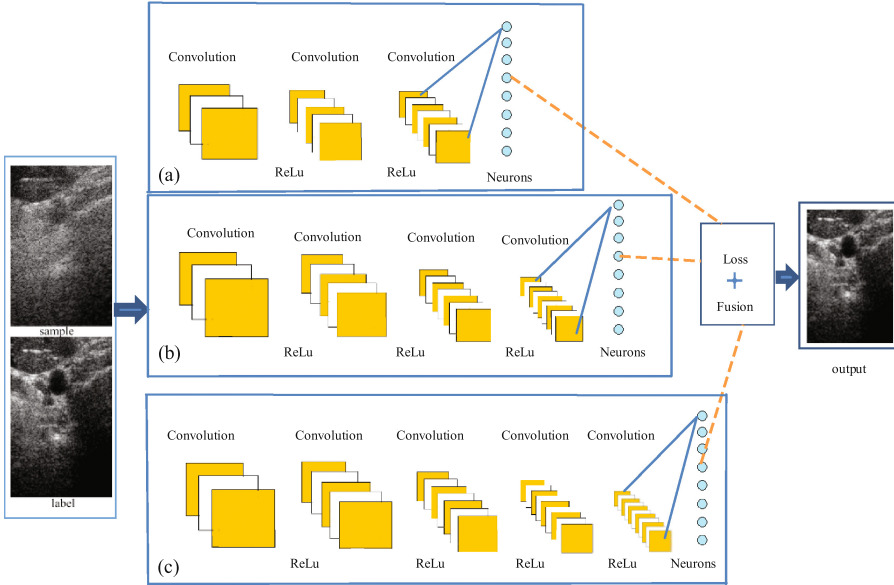
Fig. 2. The multi-scale structure. The model (a), (b) and (c) referred to as Model 1, Model 2 and Model 3.

2.3   Implementation

We implement the ultrasound super-resolution reconstruction method in MATLAB, using the MatConvNet library. In addition, a TitanX Graphic Processing Unit (GPU) was used to accelerate the CNN training speed. We selected the patch size of 31×31, 21×21 and 13×13 respectively. The patches were gained by a sliding window with the stride of 2. After data normalization, the input training pairs were convoluted layer by layer. Until the last convolution layer, the output turned into one pixel, so we generated a mapping from the low-resolution patch to the center pixel of the corresponding high-resolution patch. The fusion step was finished by computing the mean of the output pixels of three different models.

After each convolution layer, a non-linear mapping was established by a rectified linear (ReLu) function which was defined as $f(x) = max(0, x)$. The ReLu function is more biologically plausible than the widely used logistic sigmoid or hyperbolic tangent. The loss layer was calculated by minimizing the mean squared error M between the high-resolution multi-angle composite images and reconstructed images, where y and $f(x)$ denote the high-resolution images and the predict value respectively.

$$MSE = \frac{1}{2}\|(y - f(x))\|^2 \tag{1}$$

2.4   The Feedback System

By the method shown in Fig. 3, the weight of the multi-scaled network updated after each iteration. The feedback system generated outputs using the real time weight and added the outputs to the training set. During the CNN iterative process, in order to reach the convergence precision, the stochastic parallel gradient descent optimization algorithm was chosen with the batch-size of 16 and learning rate of 0.02.
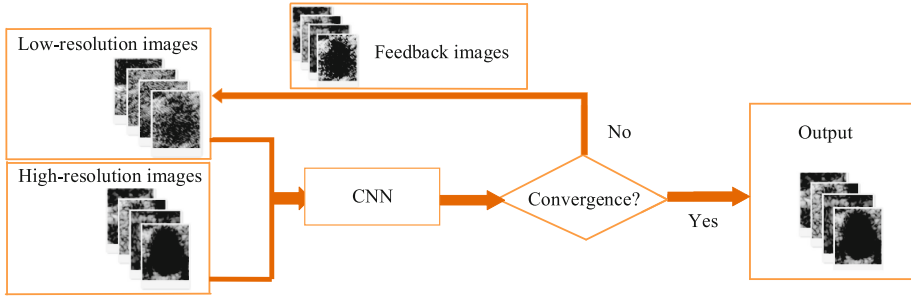

Fig. 3. The feedback system of CNN model.

3   Results

To evaluate the performance of the proposed method, we calculated the peak signal to noise ratio (*PSNR*) [13], structural similarity index measurement (*SSIM*) [14] and mutual information (*MI*) [15] for all kinds of the results. Besides, the full width at half maximum (*FWHM*) [16] and contrast ratio (*CR*) [17] were selected to measure the simulated point object images and cyst images correspondingly.

The results on the following tables were recorded with the average value of each type's 75 pairs of images and obtained using images which were not used during training. 4/5 of the data were selected as the training set, the rest of them were classified as the test set. We evaluated the performance of three different CNN models by 5-fold cross validation and the results on the tables generated by the test set only.

3.1   Reconstruction Performance on Different Target

Firstly, we compared the performance of three different CNN models with simulated images. Considering the point object images, as shown in Table 1, we found a total of 51.38% improvement in the *PSNR*, an almost five-fold increase in the *SSIM*, a 2.5-fold decrease in the *FWHM* and a small increase in the *MI*.

Table 1. Results of point object images reconstructed with Model 1.

	PSNR	SSIM	MI	FWHM
Low-resolution	24.1708	0.1962	0.4124	0.49
Reconstruction	36.5884	0.9216	0.4483	0.196

116   Z. Zhou et al.

For the cyst imaging experiment, Table 2 shows that with the gradually increasing of the template size, the *PNSR* reduced but the *SSIM* increased. Besides, when the number of CNN layers is in a certain range, the speckle quality can be preserved well. Based on these, the multi-scaled model was applied to the reconstruction problem. In Fig. 4, we visualized the reconstruction results of simulated images, by which the improvement of the images quality can be observed clearly.

Table 2. Comparison of different CNN models, taking cyst simulation images as an example, using the average PSNR, SSIM, CR and FWHM.

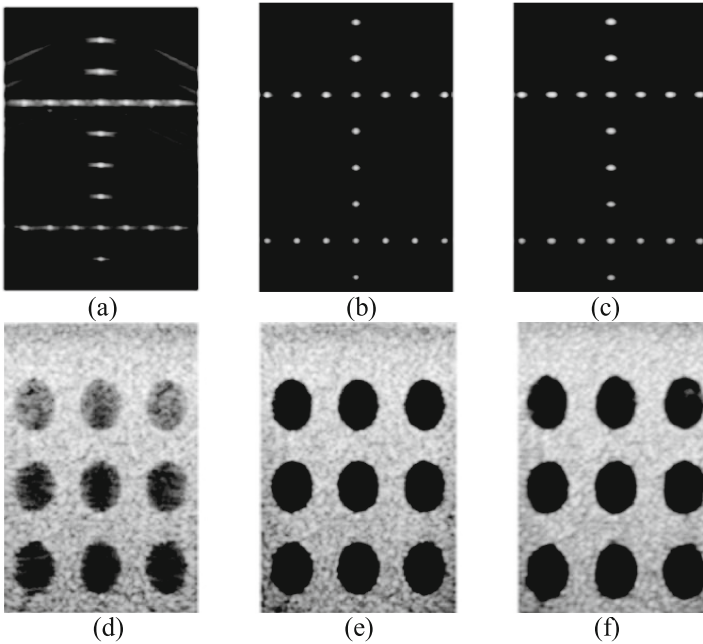|	PSNR	SSIM	MI	CR
Low resolution	15.8860	0.5537	1.1976	137.0473
Model 1	24.2301	0.5706	1.2723	166.6117
Model 2	23.1239	0.5855	1.4489	187.8386
Model 3	22.9164	0.6297	1.4831	172.3645
Multi-scaled model	24.0167	0.6135	1.5622	184.0432

Fig. 4. Result of simulation images. (a) The low-resolution point object image. (b) The high-resolution image. (c) The reconstructed point object image using Model 1. (d) The low-resolution cyst image. (e) The high-resolution cyst image. (f) The reconstructed cyst image using Model 2.

The results of phantom images are shown in Fig. 5, we found that the reconstruction results of small targets were obviously superior to the reconstruction results of large, weak-edge targets. It further concludes that a single structure may not be suitable for multi-tissue images reconstruction.
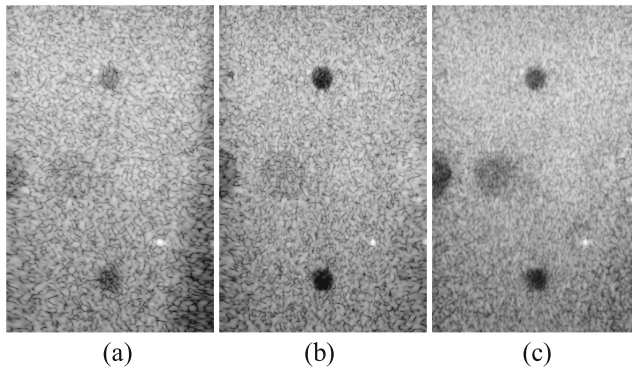
Fig. 5. Result of phantom images. (a) The low-resolution multi-tissue phantom image. (b) The high-resolution image. (c) The reconstructed image using Model 1.

3.2 Effect of Dynamic Feedback

We further evaluated the role of the dynamic feedback system in this experiment, as shown in Fig. 6 and Table 3, the reconstructed results of thyroid images with the dynamic feedback system have a considerable improvement.
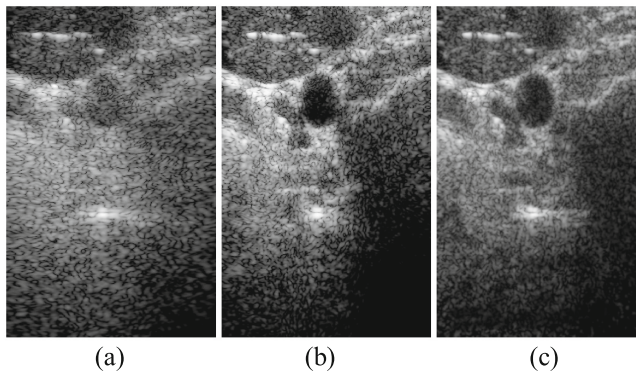

Fig. 6. Reconstructed results of thyroid images with dynamic feedback system. (a) The low-resolution image. (b) The high-resolution image. (c) The reconstructed image using the multi-scaled model.

Table 3. The effect of dynamic feedback system (take thyroid images for example).

	PSNR	SSIM	MI
Low resolution	14.9235	0.0291	0.3474
Proposed (multi-scaled)	20.1224	0.2850	0.8392
Proposed2 (with feedback system)	21.7248	0.3034	0.8856

As shown in Fig. 7, it is indicated that the feedback method can not only guarantee the global convergence, but also improve the converging rate and the stability. The method reduced roughly 15% of the total elapsed time and made the system converged to a better solution.
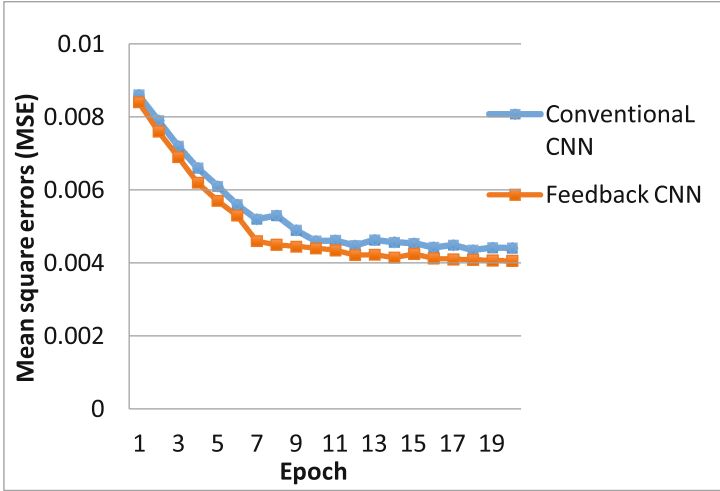

Fig. 7. Comparison of the object function.

4   Discussion

The resolution of medical imaging has a significant impact on the diagnosis of doctors, but is limited by imaging equipment and costs. With this intent, the medical image super-resolution reconstruction has been proposed and improved the image quality. As deep learning is a hot topic and is suitable to solve many different problems, we applied CNN methods to medical image super-resolution reconstruction and achieved a satisfying result.

Further research still needs to be done to convert the method to the practical application and extend to various medical image modalities. For generalization, the network structure and parameter adjustment may have a distinct impact on the results. So it could be a question how to select the appropriate network and parameters to a particular modality super-resolution reconstruction. In addition, transfer learning could be an effective mean for medical image quality elevation from training phantom image to solve the limit of image data [18]. Since the ultrasound diagnoses sometimes are based on video such as the fetal echocardiography, video super-resolution reconstruction with convolutional neural networks [19] may also be a feasible direction for further research.

5   Conclusion

In this paper, we have proposed a novel deep convolutional neural network architecture for reconstructing plane-wave ultrasound images from beamformed images, by exploiting ultrasound simulation images, phantom images and real human images. Since the experiment results show that our method generates less noise and better resolution and contrast, the performance of multi-scaled CNN model with feedback system has been proved.

References

1. Holfort, I.K., Gran, F., Jensen, J.A.: Plane wave medical ultrasound imaging using adaptive beamforming. In: Sensor Array and Multichannel Signal Processing Workshop, pp. 288–292 (2008)
2. Sasso, M., Cohen-Bacrie, C.: Medical ultrasound imaging using the fully adaptive beamformer. In: IEEE International Conference on Acoustics, Speech, and Signal Processing, pp. 489–492 (2005)
3. Zhao, J., Wang, Y., Zeng, X.: Plane wave compounding based on a joint transmitting-receiving adaptive beamformer. IEEE Trans. Ultrason. Ferroelectr. Freq. Control **62**(8), 1440–1452 (2015)
4. Kruizinga, P., Mastik, F., De, J.N.: Plane-wave ultrasound beamforming using a nonuniform fast Fourier transform. IEEE Trans. Ultrason. Ferroelectr. Freq. Control **59**(12), 2684–2691 (2012)
5. Zhou, F., Yang, W., Liao, Q.: Interpolation-based image super-resolution using multi-surface fitting. IEEE Trans. Image Process. **21**(7), 3312–3318 (2012)
6. Ji, H., Ller, C.: Robust wavelet-based super-resolution reconstruction: theory and algorithm. IEEE Trans. Pattern Anal. Mach. Intell. **31**(4), 649–660 (2008)
7. Zhao, N., Wei, Q., Basarab, A.: Single image super-resolution of medical ultrasound im-ages using a fast algorithm. In: IEEE International Symposium on Biomedical Imaging, pp. 473–476 (2016)
8. Gu, S., Zuo, W., Xie, Q.: Convolutional sparse coding for image super-resolution. In: IEEE International Conference on Computer Vision, pp. 1823–1831 (2015)
9. Dong, C., Loy, C.C., He, K.: Image super-resolution using deep convolutional networks. IEEE Trans. Pattern Anal. Mach. Intell. **38**(2), 295–307 (2016)
10. Kim, J., Lee, J.K., Lee, K.M.: Accurate image super-resolution using very deep convolutional networks. In: IEEE Conference on Computer Vision and Pattern Recognition, pp. 1646–1654 (2016)
11. Bahrami, K., Shi, F., Rekik, I.: Convolutional neural network for reconstruction of 7T-like Images from 3T MRI using appearance and anatomical features. In: Deep Learning and Data Labeling for Medical Applications, pp. 39–47 (2016)
12. Liebgott, H., Rodriguez-Molares, A., Cervenansky, F.: Plane-wave imaging challenge in medical ultrasound. In: Ultrasonics Symposium, pp. 1–4 (2016)
13. Huynh-Thu, Q., Ghanbari, M.: Scope of validity of PSNR in image/video quality assessment. Electron. Lett. **44**(13), 800–801 (2008)

14. Hore, A., Ziou, D.: Image quality metrics: PSNR vs. SSIM. In: International Conference on Pattern Recognition, pp. 2366–2369 (2010)
15. Li, J., Zhang, X., Ding, M.: Image quality assessment based on regional mutual in-formation. In: International Conference on Intelligent Computation and Bio-Medical Instrumentation, pp. 113–115 (2011)
16. Amiri, I.S., Ahmad, H., Al-Khafaji, H.M.: Full width at half maximum (FWHM) analysis of solitonic pulse applicable in optical network communication. Am. J. Networks Commun. **4**(2–1), 1–5 (2015)
17. Zhao, J., Wang, Y., Yu, J., Guo, W., Li, T., Zheng, Y.: Subarray coherence based postfilter for eigenspace based minimum variance beamformer in ultrasound plane-wave imaging. Ultrasonics **65**, 23–33 (2016)
18. Hoochang, S., Roth, H.R., Gao, M.: Deep convolutional neural networks for computer-aided detection: CNN architectures, dataset characteristics and transfer learning. IEEE Trans. Med. Imaging **35**(5), 1285–1298 (2016)
19. Kappeler, A., Yoo, S., Dai, Q.: Video super-resolution with convolutional neural net-works. IEEE Trans. Comput. Imaging **2**(2), 109–122 (2016)